

Application of micro-computed tomography to decipher deposition and flocking patterns of clogging material on cylindrical drip emitters

Venkata Ramamohan Ramachandrupa^{1,*} and Ramamohan Reddy Kasa²

¹Water and Livelihoods Foundation, Tarnaka, Secunderabad, Telangana 500 017, India

²C.V.R. College of Engineering, Mangalpalli, Ibrahimpatnam (M), Telangana 501 510, India

Five sets of cylindrical drip emitters used for up to five years in the farmlands were scanned using micro-computed tomography. Around 54.46–94.52% of the total clogging material on the emitters was found on the active outlet areas that facilitate delivery of water by the emitters. Also, larger flocks of the clogging material were found on the outlet areas. Emitter geometric features, viz. width of flow path, dent angle and boundary curvature were observed to influence the extent of physical and chemical clogging. Any attempt to design an anti-clogging emitter may necessarily include optimization of active outlets.

Keywords: Anti-clogging performance, drip emitter, flocking patterns, geometry optimization, micro-computed tomography.

CLOGGING of emitters in drip irrigation systems takes place progressively as they are used for a longer duration in the farmlands. In the case of irrigation using groundwater pumped from the wells, physical clogging due to the particles in water and chemical clogging due to the precipitation of dissolved chemicals in water are two major concerns. The hydraulic performance of an emitter diminishes due to clogging, resulting in reduced discharge.

The approach taken by various researchers to study the emitter hydraulic and clogging behaviour may broadly be classified as (i) laboratory and field experimentation, (ii) computational fluid dynamics (CFD) modelling and (iii) non-destructive analysis. Often, there is a blend of these three approaches for validating the findings. Numerical modelling has been increasingly used in recent times, often validated by laboratory experimentation and non-destructive analysis. Assessment of the hydraulic performance of locally available emitters and drip systems has been done by researchers for a long time^{1–5}. The major focus of these studies was on assessing the hydraulic performance in terms of the ability of individual emitters to deliver rated discharge and the uniformity of discharge in a drip system at a given pressure in laboratory and field settings.

This approach was later applied to study the clogging of flat-type emitters in drip irrigation systems. The reduction in rated discharge and uniformity of discharge for a given pressure in the system were used to determine the extent of clogging in the emitters. While some studies focused on physical clogging alone, others also dealt with chemical clogging due to the precipitation of dissolved chemicals in water on the emitter surface under favourable conditions. However, this conventional method of clogging studies measuring the discharge from flat emitters as a proxy in a laboratory setting neither quantifies the extent of deposition nor reveals the clogging material's deposition pattern. Few laboratory studies examined emitter clogging in relation to the pressure and discharge variations due to artificially added physical clogging material on a shorter time cycle^{6,7}. A variant of this is the study of the clogging performance of emitters when low-quality water, including treated wastewater, is applied. Feng *et al.*⁸ performed such studies, focusing more on the composite clogging behaviour of different types of emitters. Building on this approach, Yavuz *et al.*⁹ collected emitters used in the farmlands for 2–3 years and conducted clogging and hydraulic performance studies under different laboratory pressure conditions. Measurement and characterization of clogging material deposits by physical extraction, either using the ultrasonic wave method or by peeling-off using small hand tools, were done by Han *et al.*¹⁰. They compared the normal intermittent method of irrigation with the continuous irrigation method and concluded that the former method resulted in a higher degree of clogging¹⁰.

Evolution of CFD techniques facilitated visualization of flow field through the emitter flow channels, which could not be done using physical experimentation methods. Later developments in CFD also facilitated modelling the trajectory of physical particles in water through the emitter flow paths and identification of potential clogging regions. Using CFD technique, Dazhuang *et al.*¹¹ suggested 1.00 as the optimum ratio of the dentate height and flow path width of the labyrinth channel for the best hydraulic and anti-clogging emitter properties. Li *et al.*¹² used CFD and digital particle tracking velocimetry techniques to understand physical particle movement through the zig-zag flow path having rectangular dents. Weijing *et al.*¹³ optimized divided-flow

*For correspondence. (e-mail: ramamohan.ramachandrupa@gmail.com)

labyrinth-flow emitters using CFD and experimental approaches.

Yu *et al.*¹⁴ and Ouarriche *et al.*¹⁵ studied the clogging mechanism of sand particles of various sizes in relation to the geometry of labyrinth flow paths. Feng *et al.*¹⁶ focused on optimizing the flow-path boundaries for self-cleaning vortex formation in the flow field. Feng *et al.*¹⁶ and Li *et al.*¹⁷ concluded that the least cross-sectional area giving the highest flow velocity and curved boundaries, is favourable for anti-clogging properties. Yu *et al.*¹⁸, using the discrete element method (DEM) coupled with CFD, determined that a dent angle of 60°–90° is the most favourable for the anti-clogging performance of labyrinth in drip emitters. Xu and Zhang¹⁹ reduced the low-velocity vortex zones for better anti-clogging abilities of labyrinth flow paths. Yang *et al.*²⁰ optimized the labyrinth dentiform path of flat emitters by increasing the turbulent kinetic energy of water flow. Some of the above-mentioned studies validated their findings by supplementing with laboratory tests on the emitters. However, most of these studies were on flat emitters. Studies focussing on cylindrical emitters are limited. Bounoua *et al.*²¹ numerically modelled and experimentally verified the flow of clay-loaded physical clogging material through the long-path cylindrical emitters.

The application of non-destructive testing and evaluation (NDTE) methods to emitter clogging studies is an emerging area. Yanfang *et al.*²² characterized the chemical clogging material accumulated on cylindrical and flat-type emitters using a field emission scanning electron microscope (FESEM) and concluded that it predominantly consisted of calcium carbonate (CaCO₃). Ribeiro *et al.*²³ used optical microscopy techniques to study water samples and SEM techniques to study the clogging material after conducting short-cycle laboratory irrigation experiments. Using micro-computed tomography (μ CT) to segment materials with distinct X-ray properties is emerging as a promising application, especially when the materials and their patterns are hidden from examination by the naked eye or using direct observation microscopes. Nguyen and Indraratna²⁴ studied the clogging characteristics of natural fibre drains using a high-resolution μ CT technique. Xiao *et al.*²⁵ studied the biofouling patterns in different labyrinth paths of flat emitters using CT technique, when irrigated using treated wastewater. Ramachandru and Kasa^{26,27} reported the clogging patterns on used cylindrical emitters collected from farmlands using μ CT imaging. The extracted clogging material was analysed using energy-dispersive X-ray fluorescence (EDXRF) and X-ray diffraction (XRD) techniques. In a recent study, Petit *et al.*²⁸ used visible and near-infrared (vis/NIR) spectroscopy to measure the thickness of physical and chemical clogging materials on laboratory-made samples.

However, much of the earlier research was on optimizing the labyrinth flow paths alone to achieve optimum velocity field and reduce clogging. Experimental studies and physical extraction of clogging materials are inaccurate due to

their small quantities. Also, physical extraction of clogging materials disturbs the deposition pattern on the emitter surface, making it difficult to determine the relationship between emitter geometry and clogging patterns. The study of emitters that have accumulated clogging material over the years and under actual farm conditions provides useful insights about time-tested emitter clogging behaviours. μ CT is the most useful non-destructive technique to study the undisturbed clogging patterns without affecting the emitters. Also, μ CT enables accurate segmentation and quantification of clogging material from other materials of the emitter, because of its distinct X-ray attenuation properties. The present study not only quantifies the total clogging material but also relates it with different geometric areas of the emitter, such as inlets, outlets and labyrinth paths.

Materials and methods

Sampling of emitters

Five sets of cylindrical drip emitters used by farmers in their farmlands in Gundala mandal, Yadadri Bhongir district, Telangana, India, were collected from five drip systems. These systems were selected for sampling to include the emitters manufactured by different drip companies with varying geometric features and water sources. From each of these drip systems, two emitters, one from the head-end and the other from the tail-end, were cut from a randomly selected lateral pipe. Table 1 presents the sample identification, years of use and type of water source for each sample set.

Thus, a total of ten emitter samples were collected for this study, with their usage time varying from one to five years. All the sample emitters had a nominal discharge of 4 litres per hour (lph). All the sampled drip systems were provided with a screen filter of 100 μ m size. In the case of open well (OW) source, sand filters were installed as a pre-filter to the screen filter. Emitter sets 1, 2 and 3 were different from each other in terms of geometrical features of the flow path, inlet location and outlet configuration. Emitter sets 4 and 5 were identical in their geometry and usage time but had different water sources.

Table 1. Details of sample drip emitters

Sample emitter ^a	Years of use	Source of water ^b
1-1 and 1-2	4	OW
2-1 and 2-2	1	BW
3-1 and 3-2	5	BW
4-1 and 4-2	3	OW
5-1 and 5-2	3	BW

^aSample emitter is numbered in the format 'set number-emitter number'. Head-end emitters are assigned the number '1' and tail-end emitters number '2'.

^bOW, Open well; BW, Bore well.

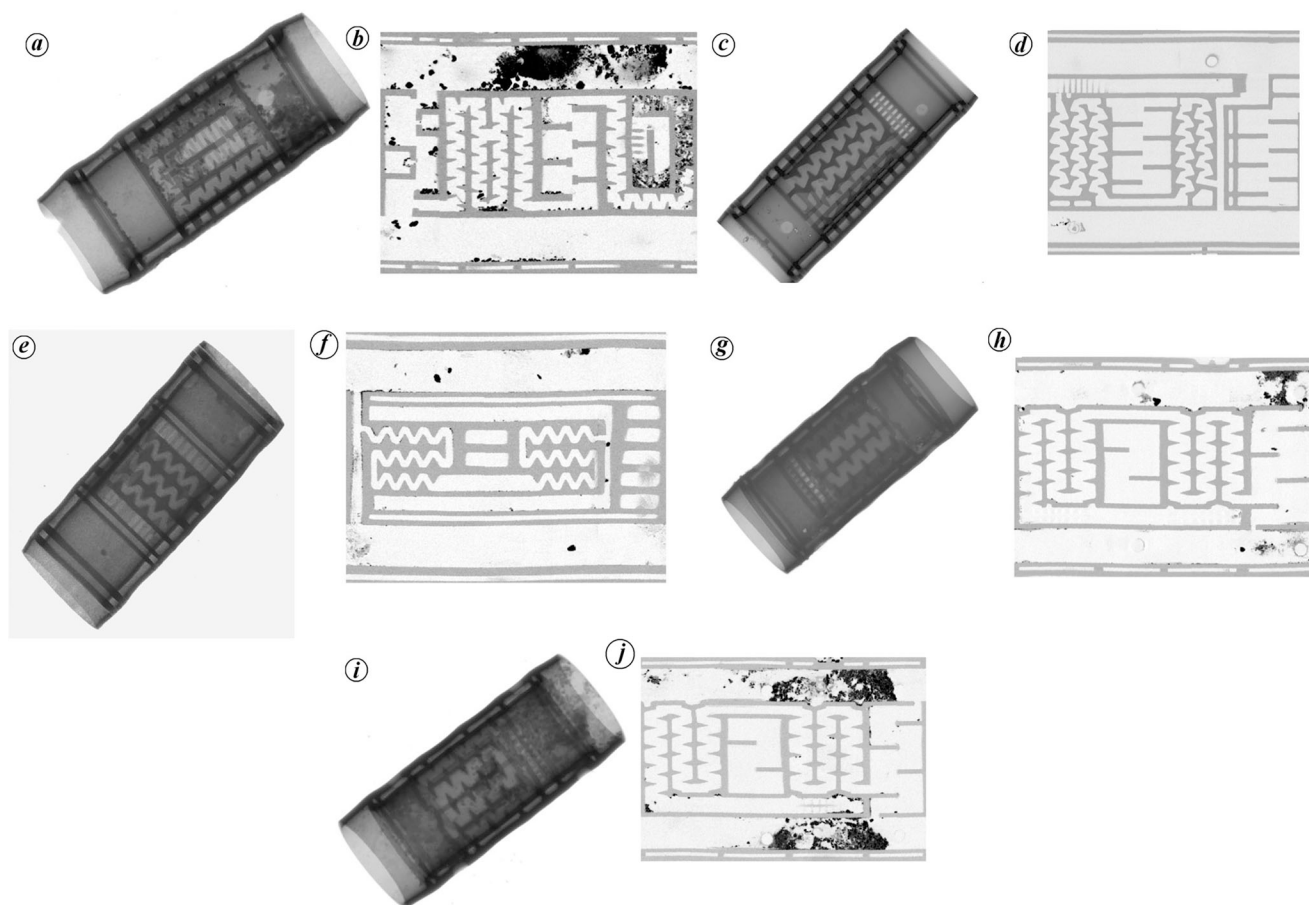


Figure 1. Three-dimensional cylindrical view and 2D unwrapped view of the five head-end sample emitters. *a, b*, Emitter 1-1; *c, d*, emitter 2-1; *e, f*, emitter 3-1; *g, h*, emitter 4-1; *i, j*, emitter 5-1.

Scanning of emitters and pre-processing

The ten sample emitters were scanned in a GE Phoenix CT machine as 16-bit 3D images at 42 μm volume element (voxel) resolution. The image data, in the form of greyscale 2D slices and 3D image channels, were visualized in Dragonfly software ver. 2021.1 (Object Research Systems Inc., Canada). The intensity assigned to each voxel in the image represents the ability of the physical material of that voxel to attenuate X-rays from passing through it. Thus, a higher intensity represents a denser material, and a lower intensity represents a relatively thinner material.

The image data contained primarily three distinct materials, viz. the emitter body, air inside the emitter paths and clogging material. The intensity of voxels ranged between 0 and 65,535, with lower-intensity voxels appearing darker and higher-intensity voxels brighter in the image. Thus, while air appeared darker in the image, the clogging material appeared the brightest of all the three materials. The intensity of the emitter body was found to be between air and clogging material. The greyscale look-up table (LUT) of voxels was inverted to facilitate clear visualization of emitter-clogging material in a darker shade.

Unwrapping images and deciphering geometric features

At the time of sampling, it was known that the emitters were manufactured by different companies with distinct geometric features. However, precise information on the orientation and dimensions of different geometric features, such as flow paths, outlet areas and inlets, was unknown. The cylindrical 3D images of drip emitters also did not permit visualizing different parts of the emitter surface and their interconnectivity simultaneously. Therefore, 3D images of the ten sample emitters were unwrapped to planar views using the SoupCanUnwrap plug-in in the Dragonfly software. The unwrapped 3D images comprised a stack of approximately 100 slices of 2D images in the XY plane, each representing the surface features of the cylindrical emitter at a given radial distance from the longitudinal axis of the emitter. The unwrapped 3D images obtained were not precisely planar due to the distortion of the sample emitters under field conditions. Figure 1 presents the 3D cylindrical view as well as one of the 2D unwrapped sectional views for each head-end sample emitters.

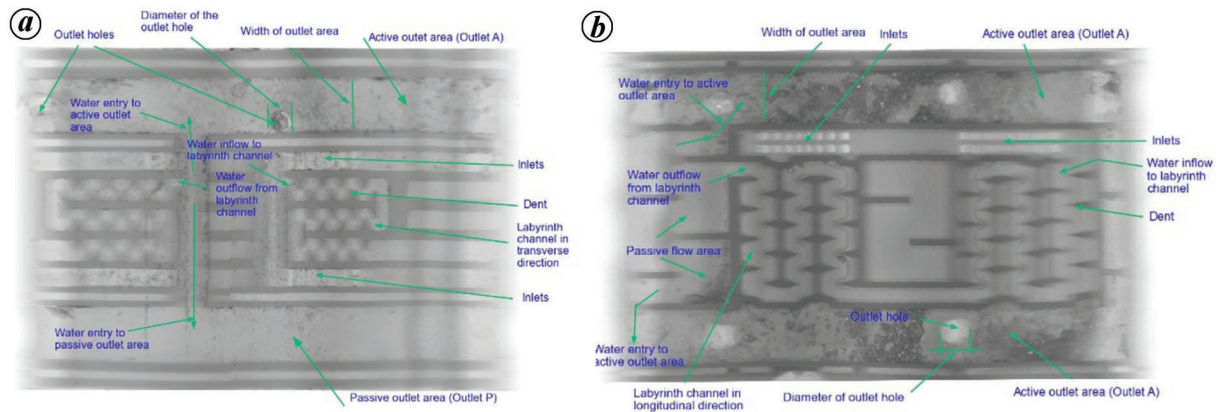


Figure 2. Different geometric features of a typical cylindrical emitter annotated on the unwrapped 3D views of sample emitters with one and two active outlets. *a*, Emitter 3-2 having one active outlet area and labyrinth path in the transverse direction. *b*, Emitter 5-2 having two active outlet areas and labyrinth path in the longitudinal direction.

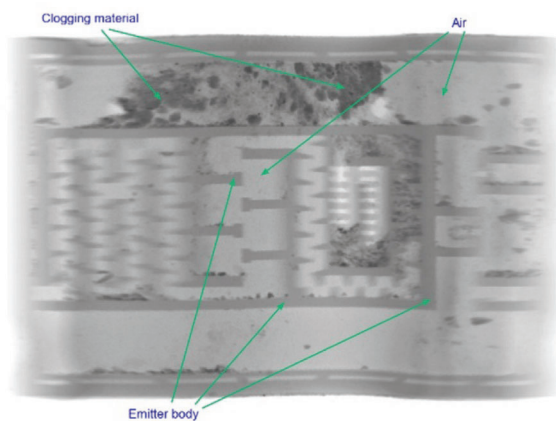


Figure 3. Emitter body, air and clogging material marked on the unwrapped emitter 1-1 in a 3D view.

The emitters sampled had distinct geometric features, primarily in terms of three aspects, viz. (i) the shape of the labyrinth channel, (ii) configuration of inlets and (iii) configuration of outlets. Each of these aspects may be further expressed in terms of a few physical geometric parameters that may be either described or measured (Figure 2). For example, the shape of the labyrinth channel is defined by the (a) dent shape and angle, (b) flow-path orientation, (c) boundary shape and (d) flow-path width. A total of nine such features were captured for each unwrapped sample emitter using the annotation and measurement features in the Dragonfly software.

Segmentation and quantification of clogging material

The clogging material on the emitter samples was segmented using the intensity threshold method in the window leveling feature of the Dragonfly software. The physical clogging material in suspension and emitter geometry interact

only after the irrigation water carrying the clogging material enters the emitter surface. Therefore, the clogging material deposited on the emitter surface alone was considered for segmentation, and the rest of the clogging material on the outer surfaces of the lateral tube was ignored.

The region of interest (RoI) files were generated that contained the clogging material separated from the 3D images. These RoIs were further clipped and separated into three sub-RoIs, viz. clogging material on the outlet areas, labyrinth flow paths and inlet areas respectively. While retaining the colour LUT of the air and emitter body in the inverted greyscale, the clogging materials on different parts were assigned different pseudo colours to distinguish them clearly. The volume of clogging material in each of these three geometric areas was quantified from the three sub-RoIs. Further, volume-based distribution of clogging material accumulation on different parts of the sample emitters was done using the connected component analysis feature in the Dragonfly software. The volume distribution histograms and volume-based segmentation images were used to interpret the particle flocking and growth pattern of clogging material patches with time.

Results

Composition of emitters in the scanned images

The scanned 3D images and their 2D slices in the *XY*, *YZ* and *XZ* planes provided information about the composition of each sample emitter. Typically, the samples contained three distinct physical materials, viz. (i) the emitter body made of polyethylene, (ii) air occupying the open spaces, and (iii) clogging material spread on the surface of the emitter. Figure 3 depicts these materials in a 3D unwrapped view of emitter 1-1. Since the greyscale intensity values were inverted, the clogging material appeared in a distinct darker colour.

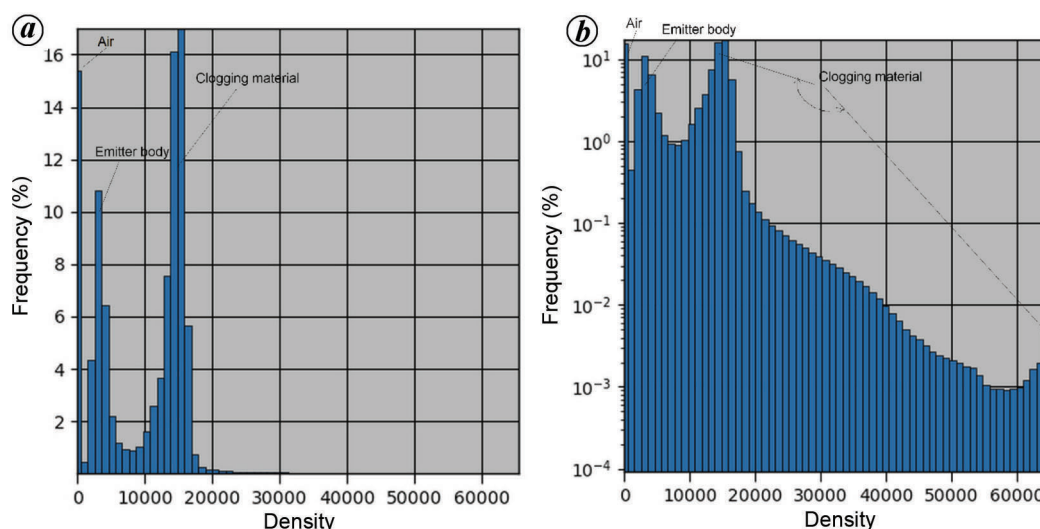


Figure 4. Frequency histograms of voxel intensity of sample emitter 4-1 annotated identifying air, emitter body and clogging material. *a*, Linear scale; *b*, logarithmic scale.

Table 2. Geometric features and measured dimensions of sample emitters

Sample emitter set	Shape of labyrinth channel			Channel width (mm)	Number and location of inlets		Configuration of outlets		
	Dent shape and angle	Flow path orientation ^a	Boundary shape		Number and position of inlets	Sectional area perpendicular to the flow (mm ²)	Width of outlet area (mm)	Number and position of outlet holes	Diameter of the outlet hole (mm)
1	Right-angled, curved tip, 17.6°	Longitudinal	Linear edges	0.94–1.12	One, middle of the emitter	47.68	5.84	Two, on one side of the emitter	2.02
2	Triangular, curved tip, 32.0°	Longitudinal	Sloping edges with curved corners	1.12–1.25	Two, on one side of the emitter	42.17	5.33	Two, one each on either side of the emitter	1.71
3	Triangular, curved tip, 56.4°	Transverse	Curved edges and corners	0.81–1.09	Four, two on either side of the emitter	64.82	5.77	Two, on one side of the emitter	2.34
4 and 5	Triangular, sharp tip, 31.1°	Longitudinal	Linear edges with curved corners	1.28–1.51	Two, on one side of the emitter	44.06	4.82	Four, two on either side of the emitter	2.19

^aThe direction of labyrinth flow path that carries water from inlet to outlet of the emitter is differentiated with reference to the direction of flow in the lateral tube.

The emitter body was manufactured using machines to the pre-defined geometric size and shape. In contrast, the clogging material accumulated over a period of time, growing in irregular shapes and patterns. Thus, these two could easily be distinguished from one another. The X-ray intensity of air was in the range of 0–12,091. The polyethylene material had the X-ray intensity range of 5,927–24,499 for different emitter samples. The wider range of intensity for polyethylene could be due to the variations in raw material, the process of manufacture by different drip irrigation companies, and differences in the density of the emitters. The clogging material, which is the material of interest in this study, was found to have intensity values in a wide range of 13,747–65,535. However, for a given emitter, there was no overlap of intensity of the three materials.

The intensity histograms of the emitter images clearly distinguish between air, emitter body and clogging material, each separated by valleys between peaks. Figure 4 *a* and *b* present the intensity histograms of sample emitter 4-1, with the frequency of voxel X-ray intensity on *Y*-axis shown on the linear and logarithmic scales respectively. The presence of clogging material is not highlighted when plotted on a linear scale, as its volumetric proportion relative to that of the emitter body is small. The clogging material distribution is clearly seen when the frequency is plotted on a logarithmic scale. Clogging material is spread over a wide range of intensity values, though the fraction of higher-intensity clogging material is much smaller. This wide range of intensity values in the case of clogging material could be because the particles get randomly accumulated

over a longer period, unlike the emitter body manufactured from a chosen physical material.

Geometric features of sample emitters

The emitters sampled possessed distinct geometric features that have a bearing on the dynamics of water flow through them. The shape of the labyrinth channel, defined by the dents, boundary curvature and channel width, was unique for the sample emitters 1, 2, 3 and 4/5. The emitters also differed in terms of number and location of inlets/outlets. Table 2 summarizes these geometric features in a concise form. Since emitters 4 and 5 are geometrically identical, their details are presented together.

Emitter 3 had the highest dent angle of 56.4° , facilitating a smoothly curved transition of the labyrinth channel boundary. Also, the predominant flow direction in the labyrinth was transverse, while all other samples had longitudinal flow. This facilitated a longer flow path in a smaller surface area. The width of the labyrinth channel varied for all the samples, least for the straight channel segments, but increased whenever the channel changed its direction of flow. Emitter 3 had the smallest flow path width.

Different emitter samples had one, two or four inlets, with their locations also varying. Emitter 1 had one inlet uniquely located in the middle of the cylindrical surface, but the rest had them spread out in multiple numbers, located on either side of the labyrinth flow channel area. The cross-sectional area of inlets of samples 1, 2, 4 and 5 was in the close range 42.17–47.68 sq. mm. Again, emitter 3 stood out with a much larger inlet area of 64.82 sq. mm, divided between four inlets.

While emitters 4 and 5 had four outlets, the rest had only two. Emitters 1 and 3, though they had outlet areas on both ends, active outlet holes for water discharge were found only at one end. Emitter 2 stood out with two active outlet areas on either side with one outlet hole each. Thus, the outlet areas on both ends were active in the case of emitters 2, 4 and 5. The diameter of the outlet hole was noticeably small for emitter 2 and largest for emitter 3. However, emitters 4 and 5 had the highest gross cross-sectional area of outlet holes due to double the number of outlets holes compared to the other emitters.

Quantification of clogging material in different parts of the emitters

The segmentation of clogging material from the air and emitter body separated the voxels associated with the clogging material from rest of the voxels in the scanned images. Disaggregating the segmented voxels on four distinct regions of the emitter surface led to the volumetric quantification of clogging material on each.

The active outlet area through which water discharge takes place was designated as ‘outlet A’. The passive outlet

area had no outlet holes for water discharge and was designated as ‘outlet P’. Figure 5 shows the segmented clogging material by artificially colouring it using distinct colours on different geometric parts of all the sample emitters. Table 3 presents the clogging material quantified on outlet A, outlet P, inlet area and flow path for each emitter sample.

The amount of clogging material accumulated on the emitters is a function of their usage time in the farmlands. In the sample emitter sets, emitter had the least usage time of one year and emitter 3 had the longest usage time of five years (Table 1). Accordingly, the total quantity of clogging material found on the sample emitters varied widely from 1.054 to 89.752 mm³. Sample emitter 3, with the longest usage time of five years, accumulated less clogging material than sample emitters 1, 4 and 5. Thus, it may be inferred that the emitter geometry has a role in the degree of deposition of clogging material. Also, the amount of clogging material found on the tail-end emitters is significantly lower than that on the head-end emitters for majority of the sample emitters.

Growth behaviour of clogging material patches

The connected component analysis of the clogging material RoIs revealed the volume distribution of clogging material patches on different parts of the sample emitters. Figure 6 illustrates the volume-based segregation of clogging material patches for the five tail-end sample emitters. The patches are shown in different artificial colours based on their volume. The clogging material particles accumulated over time by flocking to each other to form patches of varying volumes. The histograms of these accumulated patches for the five tail-end sample emitters are also shown in Figure 7, presenting volume (mm³) on the *X*-axis and frequency on the *Y*-axis in a logarithmic scale. Larger volume patches were found mostly on the outlet areas, while other areas were found with dispersed clogging material patches of small volume. The disproportionately higher volume of clogging material patches on the outlet areas is seen in Figure 6*b*, even in the early years of use in the case of sample emitter 2. Emitters 1, 3, 4 and 5, with relatively more usage time, are found with much larger patches of clogging material on the outlets (Figure 6*a, c–e* respectively). A similar trend is observed in the case of head-end sample emitters.

Discussion

For all the sample emitters, it is clear that a major proportion of total clogging material gets deposited in the outlet areas. Further, for emitters 4 and 5, with two active outlet areas on either side and four outlet holes, the proportion of clogging material found on the outlet areas is the highest, in the range of 70.35–94.52%. Emitter 3 stands out with a significantly lesser volume of clogging material on the entire emitter as well as on the active outlets. The higher cross-sectional

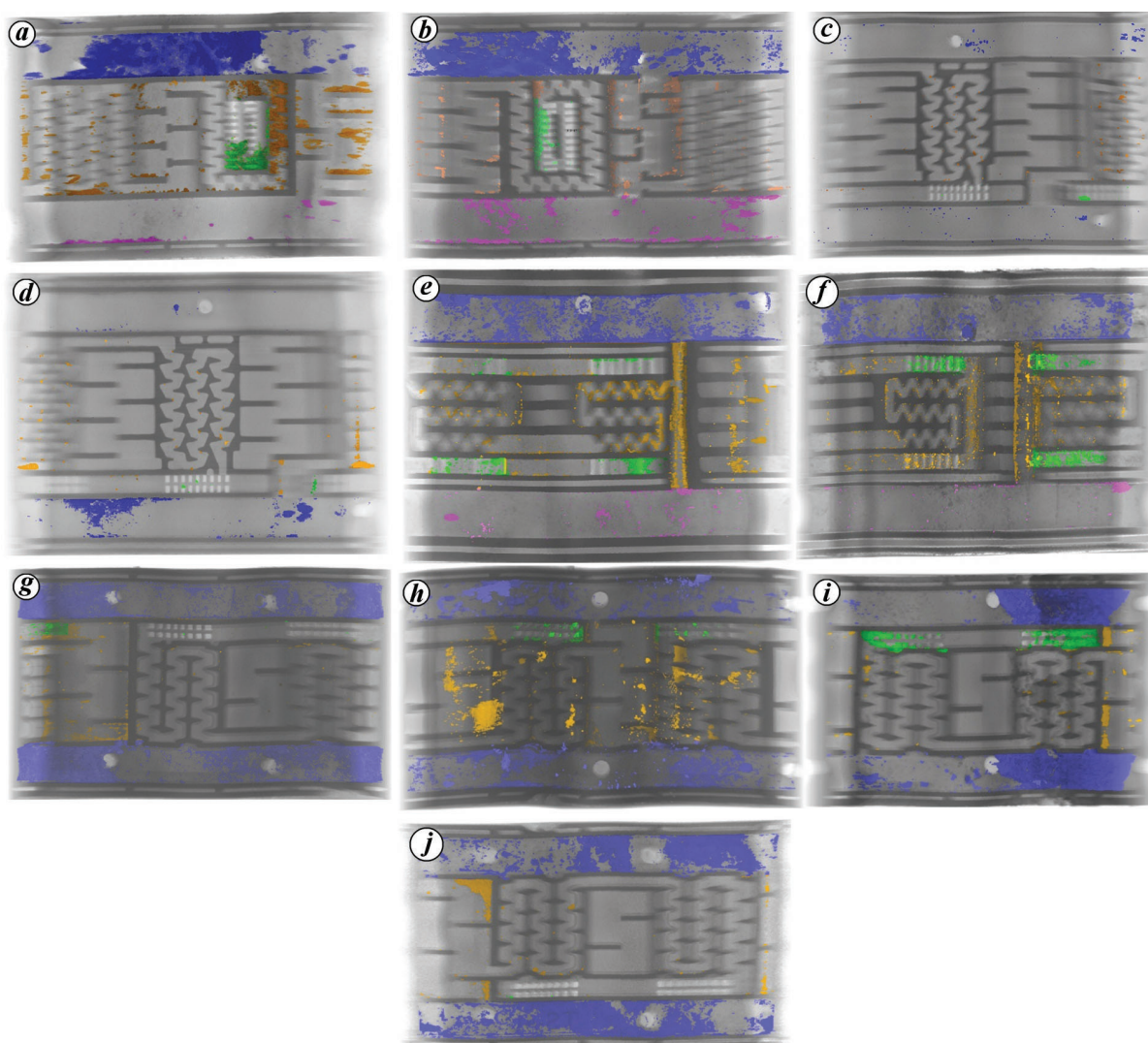


Figure 5. Clogging material segmented on different geometric areas of sample emitters in 3D unwrapped view. *a*, Emitter 1-1; *b*, emitter 1-2; *c*, emitter 2-1; *d*, emitter 2-2; *e*, emitter 3-1; *f*, emitter 3-2; *g*, emitter 4-1; *h*, emitter 4-2; *i*, emitter 5-1; *j*, emitter 5-2.

Table 3. Volume of clogging material on different geometric parts of the sample emitters

Emitter sample	Volume (mm ³) and percentage ^a of clogging material				
	Entire emitter surface	Outlet A	Outlet P ^b	Inlet area	Flow path
1-1	89.752	63.401 (70.64)	2.885 (3.21)	6.528 (7.27)	16.943 (18.88)
1-2	48.933	36.665 (74.93)	4.539 (9.28)	2.418 (4.94)	5.311 (10.85)
2-1	1.054	0.574 (54.46)	–	0.154 (14.61)	0.326 (30.93)
2-2	6.284	5.259 (83.69)	–	0.095 (1.51)	0.930 (14.80)
3-1	26.987	16.748 (62.06)	1.173 (4.35)	1.624 (6.02)	7.442 (27.58)
3-2	13.139	6.159 (46.88)	0.731 (5.56)	2.102 (16.00)	4.147 (31.56)
4-1	41.587	38.083 (91.57)	–	0.69 (1.66)	2.814 (6.76)
4-2	22.504	15.831 (70.35)	–	1.016 (4.51)	5.657 (35.73)
5-1	86.130	79.066 (91.80)	–	5.157 (5.99)	1.907 (2.21)
5-2	56.040	52.971 (94.52)	–	0.014 (0.025)	3.055 (5.45)

^aFigure in parentheses is percentage of the total clogging material. ^bThere are no passive outlet areas in case of sample emitters 2, 4 and 5.

area of inlets and narrower flow paths of emitter 3 might have kept the clogging particles in suspension beyond the outlet areas and expelled them along with water drops through the outlet holes. This observation agrees with the

findings of Feng *et al.*¹⁶ and Li *et al.*¹⁷, that the narrow curved boundaries of labyrinth flow paths augment the self-cleaning abilities of the emitters. Further, this observation about emitter 3 confirms the finding of Yu *et al.*¹⁸

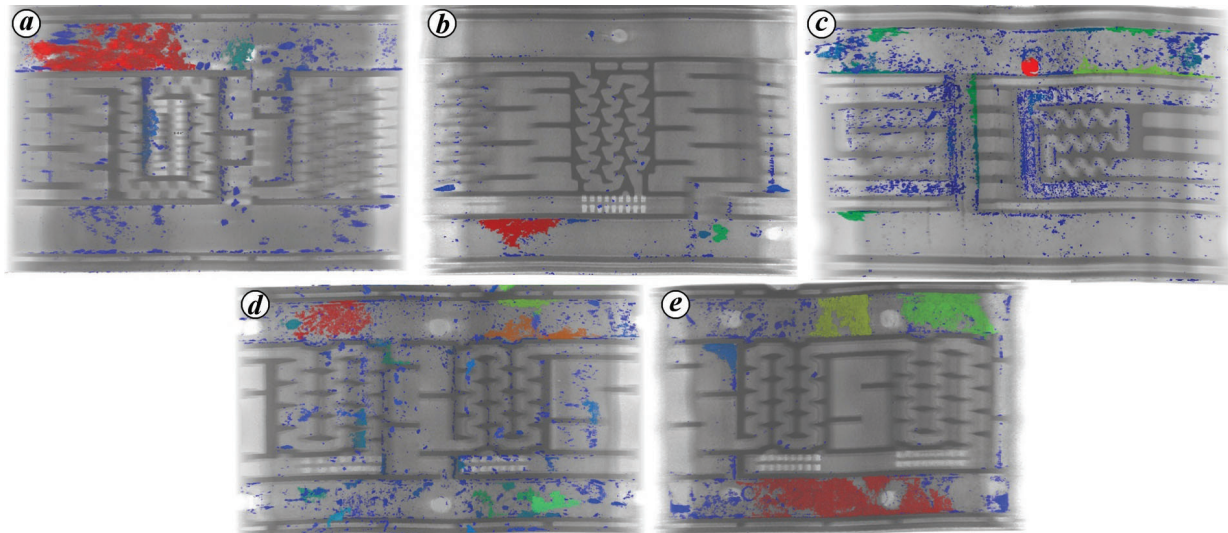


Figure 6. Volume-based segregation of clogging material patches on the five tail-end sample emitters. *a*, Emitter 1-2; *b*, emitter 2-2; *c*, emitter 3-2; *d*, emitter 4-2; *e*, emitter 5-2.

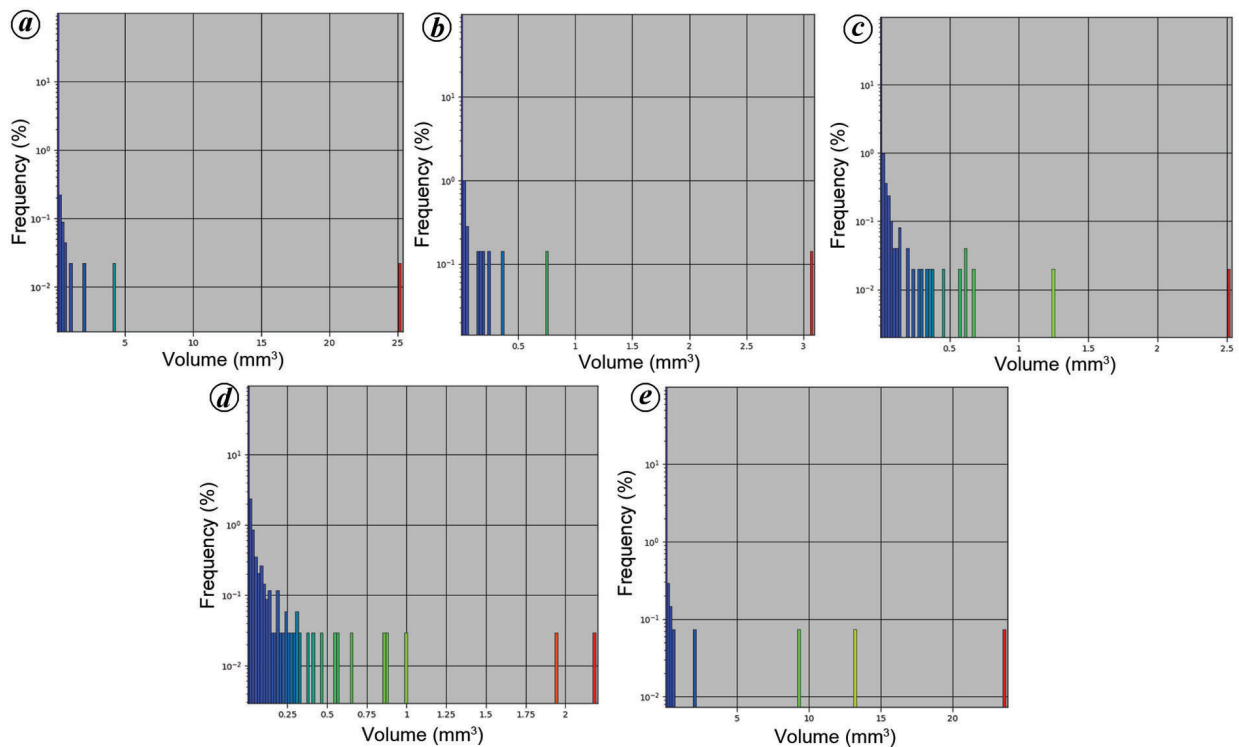


Figure 7. Volume histograms of clogging material patches on the five tail-end sample emitters. *a*, Emitter 1-2; *b*, emitter 2-2; *c*, emitter 3-2; *d*, emitter 4-2; *e*, emitter 5-2.

that higher dent angles are favourable for the anti-clogging performance of the emitters. Also, the absence of a passive flow area on the emitter 3 geometry might have helped in conserving the kinetic energy of flow water and better anti-clogging performance. Many earlier efforts of optimizing emitter geometry for reduced clogging focused on only redesigning the labyrinth flow paths of flat emitters. For a cylindrical emitter, the present study reveals that the clog-

ging material deposition on active outlets is also a matter of concern, apart from on the labyrinth paths. The amount of clogging material on the flow paths is less than that on the active outlet areas and far lower in quantity.

The volume of clogging material found on outlet P in the case of emitters 1 and 3 was small compared to that on outlet A. Though water enters both, exposure of active outlet A to the ambient atmosphere through the outlet holes

differentiates it from outlet P. The finding of Han et al.¹⁰ of higher clogging due to intermittent irrigation method is relevant to this observation. The no-flow periods between irrigations exposed the water that remains stagnant in the active outlet area to the environment, possibly accelerating the chemical precipitation of clogging materials²⁶. The diameter of each outlet hole was larger for emitter 3, but the gross cross-sectional area of the outlet holes was more for emitters 4 and 5 due to double the number of outlet holes. This leads to the inference that more exposure of outlet areas to ambient atmospheric conditions may result in more deposition of clogging material. However, the role played by air temperature, sunlight and ambient atmosphere on the extent of deposition of chemical clogging material needs a separate and specialized study. The advantages or disadvantages of having distributed outlet holes with a larger gross cross-sectional area also require laboratory studies to observe their bearing on the discharge quantity and uniformity.

A physical particle in suspension in flowing water may settle down and flock to the existing deposit of the clogging material. This growth of each patch of the clogging material by flocking to the already stuck deposit takes place progressively over time. Some particles may be dislodged by the flowing water and deposited elsewhere downstream. The study of sample emitters of different usage times revealed this growth pattern of the clogging material volume patches. A higher proportion of clogging material on the outlets in the case of emitters 1, 2, 4 and 5 indicates the ability of labyrinth flow paths to flush out physical clogging particles. However, the heavier particles might have accumulated in the outlet areas, while some lighter particles are excreted along with water through the outlet holes. Thus, larger volume patches are found on the outlet areas than on the other parts of the emitters. Lower amount of total clogging material on the sample emitter 3 indicates the efficient overall flushing ability of this emitter despite its use for the longest period of time.

Conclusion

The application of μ CT technique to study long-use drip emitters has given useful insights into the spread of clogging material on different emitter parts, which is not possible using conventional methods.

Narrower labyrinth flow paths with curved boundaries, larger inlet cross-sectional area, a larger angle at the dent tip, absence of passive flow areas and larger but fewer outlet holes are favourable geometric features for the anti-clogging performance of the emitters.

The volume proportion and flock size of clogging material accumulated on the active outlet areas are the highest for all the emitter samples. Therefore, efforts to optimize the emitter design for reduced clogging need to redesign not only the labyrinth flow channel but also the outlet geometry.

1. Kirmak, H., Dogan, E., Demir, S. and Yalcin, S., Determination of hydraulic performance of trickle irrigation emitters used in irrigation systems in the Harran plain. *Turk. J. Agric. For.*, 2004, **28**, 223–230.
2. Patil, S. S., Nimbalkar, P. T. and Joshi, A., Hydraulic study, design and analysis of different geometries of drip irrigation emitter labyrinth. *Int. J. Eng. Adv. Technol.*, 2013, **2**, 455–462.
3. Kusre, B. C. and Liansangpui, F., Assessment of hydraulic performance of drip emitters for adoption in hilly terrain of north-eastern region of India. *Irrig. Drain.*, 2016, **65**(4), 469–479.
4. Mostafa, H. and Sultan, W., Hydraulic evaluation of locally modified emitter under laboratory conditions. *J. Water Supply: Res. Technol.-Aqua.*, 2018, **67**(3), 291–296.
5. Khalil, T. M., Ajmal, M., Khan, T. A., Haq, Z. U., Khattak, M. S. and Malik, A., Evaluating hydraulic performance of locally available drip emitters used in Pakistan. *Sarhad J. Agric.*, 2020, **36**(1), 185–191.
6. Wei, Q., Shi, Y., Lu, G., Dong, W. and Huang, S., Rapid evaluations of anticlogging performance of drip emitters by laboratory short-cycle tests. *J. Irrig. Drain. Eng.*, 2008, **134**(3), 298–304.
7. de Camargo, A. P., Molle, B., Tomas, S. and Frizzone, J. A., Assessment of clogging effects on lateral hydraulics: proposing a monitoring and detection protocol. *Irrig. Sci.*, 2014, **32**, 181–191.
8. Feng, J., Li, Y., Liu, Z., Muhammad, T. and Wu, R., Composite clogging characteristics of emitters in drip irrigation systems. *Irrig. Sci.*, 2019, **37**, 105–122.
9. Yavuz, M. Y., Demirel, K., Erken, O., Bahar, E. and Deveciler, M., Emitter clogging and effects on drip irrigation systems performances. *Afr. J. Agric. Res.*, 2010, **5**(7), 532–538.
10. Han, S., Li, Y., Zhou, B., Liu, Z., Feng, J. and Xiao, Y., An *in situ* accelerated experimental testing method for drip irrigation emitter clogging with inferior water. *Agric. Water Manage.*, 2019, **212**, 136–154.
11. Dazhuang, Y., Peiling, Y., Shumei, R., Li, Y. and Tingwu, X., Numerical study on flow property in dentate path of drip emitters. *N.Z. J. Agric. Res.*, 2007, **50**, 705–712.
12. Li, Y., Yang, P., Xu, T., Ren, S., Lin, X., Wei, R. and Xu, H., CFD and digital particle tracking to assess flow characteristics in the labyrinth flow path of a drip irrigation emitter. *Irrig. Sci.*, 2008, **26**, 427–438.
13. Weijing, Y., Zhengying, W., Huali, C. and Shengli, M., Optimal design and experiment for divided-flow emitter in drip irrigation. *Trans. Chin. Soc. Agric. Eng.*, 2014, **30**(17), 117–124.
14. Yu, L., Li, N., Long, J., Liu, X. and Yang, Q., The mechanism of emitter clogging analyzed by CFD–DEM simulation and PTV experiment. *Adv. Mech. Eng.*, 2018, **10**(1), 1–10.
15. Ouarriche, H., Bouhali, M. E., Bouisfi, F., Caoui, M. and Hannaoui, M., Numerical simulation of flow in trapezoidal labyrinth-channels of drip irrigation. *FME Trans.*, 2021, **49**(1), 147–153.
16. Feng, J., Li, Y., Wang, W. and Xue, S., Effect of optimization forms of flow path on emitter hydraulic and anti-clogging performance in drip irrigation system. *Irrig. Sci.*, 2018, **36**, 37–47.
17. Li, Y., Feng, J., Xue, S., Muhammad, T., Chen, X., Wu, N., Li, W. and Zhou, B., Formation mechanism for emitter composite-clogging in drip irrigation system. *Irrig. Sci.*, 2019, **37**, 169–181.
18. Yu, L., Li, N., Liu, X., Yang, Q., Li, Z. and Long, J., Influence of dentation angle of labyrinth channel of drip emitters on hydraulic and anti-clogging performance. *Irrig. Drain.*, 2019, **68**, 256–267.
19. Xu, T. and Zhang, L., Influence and analysis of structure design and optimization on the performance of a pit drip irrigation emitter. *Irrig. Drain.*, 2020, **69**, 633–645.
20. Yang, B., Wang, J., Zhang, Y., Wang, H., Ma, X. and Mo, Y., Anti-clogging performance optimization for dentiform labyrinth emitters. *Irrig. Sci.*, 2020, **38**, 275–285.
21. Bounoua, S., Tomas, S., Labille, J., Molle, B., Granier, J., Haldenwang, P. and Izzati, S. N., Understanding physical clogging in drip

- irrigation: *in situ*, in-lab and numerical approaches. *Irrig. Sci.*, 2016, **34**, 327–342.
22. Yanfang, L., Pute, W., Delan, Z., Lin, Z. and Junying, C., Effect of water hardness on emitter clogging of drip irrigation. *Trans. Chin. Soc. Agric. Eng.*, 2015, **31**, 95–100.
23. Ribeiro, M. D., Carlos Azevedo, A. D., Santos, D. B. D., Szeikut, F. D., Klein, M. R. and Reis, C. F., Optical microscopy and SEM for identifying clogging material in a drip irrigation system. *Rev. Caatinga*, 2018, **31**(4), 997–1007.
24. Nguyen, T. T. and Indraratna, B., Micro-CT scanning to examine soil clogging behavior of natural fiber drains. *J. Geotech. Geoenviron. Eng.*, 2019, **145**(9), 1–16.
25. Xiao, Y., Sawicka, B., Liu, Y., Zhou, B., Hou, P. and Li, Y., Visualizing the macroscale spatial distributions of biofilms in complex flow channels using industrial computed tomography. *Biofouling*, 2020, **36**(2), 115–125.
26. Ramachandrupa, V. R. and Kasa, R. R., Non-destructive characterization of physical and chemical clogging in cylindrical drip emitters. *Heliyon*, 2020, **6**, e05327:1–11.
27. Ramachandrupa, V. R. and Kasa, R. R., Deep learning segmentation of clogging patterns of cylindrical drip emitters with varied geometric features. *J. Irrig. Drain. Eng.*, 2022, **148**(4), 04022006:1–9.
28. Petit, J., Mouhed, N. A., Garcia, S. M., Metz, M., Molle, B. and Bendoula, R., Potential of visible/near infrared spectroscopy coupled with chemometric methods for discriminating and estimating the thickness of clogging in drip-irrigation. *Biosyst. Eng.*, 2021, **209**, 246–255.

ACKNOWLEDGEMENT. We thank Indian Institute of Technology, Kharagpur for help in scanning the emitter samples using μ CT scanning equipment and Object Resource Systems (ORS), Canada for providing the non-commercial license of Dragonfly software.

Received 19 July 2022; accepted 12 January 2023

doi: 10.18520/cs/v124/i6/738-747